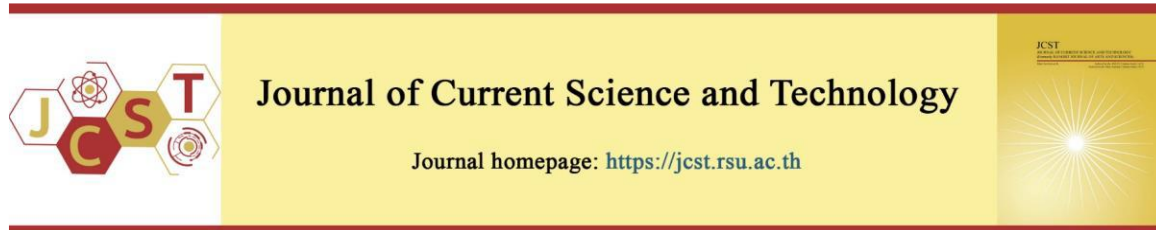


Cite this article: Nassor, S. H., Matlan, S. J., Taha, N. A., & Mukhlisin, M. (2025). Influence of hydraulic properties on the slope stability of unsaturated soil from the garinono formation in sabah. *Journal of Current Science and Technology*, 15(1), Article 88. <https://doi.org/10.59796/jcst.V15N1.2025.88>



Influence of Hydraulic Properties on the Slope Stability of Unsaturated Soil from the Garinono Formation in Sabah

Suleiman Haji Nassor¹, Siti Jahara Matlan^{1,*}, Nazaruddin Abdul Taha¹, and Muhammad Mukhlisin²

¹Civil Engineering Program, Faculty of Engineering, Universiti Malaysia Sabah, 88400 Kota Kinabalu, Sabah, Malaysia

²Department of Civil Engineering, Polytechnic Negeri Semarang, Indonesia

*Corresponding author; E-mail: jahara@ums.edu.my

Received 12 December 2023; Revised 29 April 2024; Accepted 24 October 2024; Published online 23 December 2024

Abstract

This study investigates the hydraulic response and stability of silty clays from the Garinono Formation during the rainy season, utilizing peak monthly rainfall data recorded over a decade by the Department of Irrigation and Drainage, Sabah. The research focuses on the impact of rainfall infiltration on slope stability under extreme hydrological conditions, modelled using a 31-day antecedent rainfall event from January 2011. The study incorporates both field and laboratory data, assessing the Soil-Water Characteristic Curve (SWCC) and bulk density for three distinct soil samples: (i) MI (Intermediate Plasticity Silt), (ii) ML (Low Plasticity Silt), and (iii) CI (Intermediate Plasticity Clay). The SWCC and hydraulic properties were characterized using the Fredlund, & Xing (1994) model, with subsequent numerical simulations conducted using GEO-SLOPE International. Results indicated that sample (ii) ML exhibited increased cumulative water volume with rising rainfall intensity, influenced by its saturated and unsaturated hydraulic conductivity, as well as the FX model's fitting parameter n . The study revealed that high q/K_s ratios in samples (i) MI and (iii) CI led to greater runoff and reduced infiltration, characterized by lower water storage and higher discharge rates. Conversely, lower q/K_s ratios in sample (ii) ML facilitated infiltration, increasing water storage and reducing discharge rates. A notable decrease in matric suction was observed during rainfall, with sample (ii) ML showing the most significant reductions, leading to early and substantial decreases in the Factor of Safety (FS), indicating potential instability. In contrast, samples (i) MI and (iii) CI maintained higher stability due to negative Pore-Water Pressure (PWP) and minimal suction reductions. These findings underscore the critical influence of soil permeability on slope hydrological response and stability during intense rainfall events. This study contributes to the understanding of the hydro-mechanical behaviour of the Garinono Formation, with implications for geotechnical design and slope stability analysis in tropical regions.

Keywords: *Garinono Formation; numerical slope stability analysis; rainfall infiltration; silty clay; unsaturated soil*

1. Introduction

The hydraulic characteristics of unsaturated soils are fundamental in determining how rainfall and irrigation affect soil water storage, evapotranspiration, and drainage (Huong, & Thu, 2024). These characteristics are governed by the relationship between matric potential (ψ) and soil water content (θ), as captured by the soil water retention curve (SWRC) and hydraulic conductivity function (Khlosi

et al., 2008). Understanding these properties is crucial, especially in regions prone to slope failures triggered by rainfall infiltration.

Rainfall infiltration plays a significant role in reducing matric suction and weakening soil shear strength, leading to slope instability through seepage effects (Zhou, & Qin, 2022). The complexity of these processes, influenced by nonlinear hydraulic soil properties and varying rainfall patterns, necessitates a

detailed study of how pore water pressure affects deformation in unsaturated slopes (Garcia Aristizabal et al., 2011). Key factors such as soil water retention, hydraulic conductivity, and AEV critically influence the hydro-mechanical behaviours of unsaturated soils (Kechik et al., 2023; Zaky, & Seboong, 2017).

In tropical climates, particularly in regions with residual soils like Sabah, Malaysia, rainfall-induced slope instabilities are frequent (Yunusa et al., 2014). The unique properties of tropical soils, such as their pore structure and matric suction, make them particularly susceptible to slope failures. These soils require specialized geotechnical approaches to ensure stability (Ray et al., 2023; Carvalho, & Gitirana, 2021). Typically, in such regions, the groundwater table is deep below the surface, leaving the overlying soil unsaturated and reliant on matric suction for slope stability (Yunusa et al., 2014).

Numerical methods, such as Finite Element and Finite Difference Methods, have been extensively employed to model seepage flow and slope stability in unsaturated soils (Kumar, & Roy, 2023). Studies by Mahmoud et al. (2021) and Sazzad et al., (2015) have demonstrated the effectiveness of these methods in simulating the complex interactions within slopes under varying moisture conditions, providing valuable insights into potential failure mechanisms.

Yang, and Huang (2023) and Ng, and Shi (1998) have both underscored the importance of understanding how transient seepage and infiltration patterns influence slope stability, particularly highlighting the critical role of relative compaction and pore water pressure changes. These studies, along with others by Xue et al., (2016) and Yuan et al., (2020), have shown that increased pore water pressure and reduced matric suction during prolonged rainfall are key contributors to slope instability.

Despite these advances, the specific impacts of these factors on the Garinono Formation in East Sabah remain underexplored. The Garinono Formation, characterized by chaotic deposits and Mélange soils with high plasticity, presents unique challenges for slope stability, particularly under heavy rainfall conditions (Chung et al., 2015; Musta et al., 2019).

2. Problem Statement and Objectives

The Garinono Formation in East Sabah is comprised of Mélange soils, which are classified as intermediate to high plasticity. These soils are prone to slope failure due to their loose particle composition and high moisture absorption, which leads to reduced shear strength, especially in the presence of cracks and

fissures (Musta et al., 2019). The sensitivity of these soils to wet-dry cycles exacerbates their instability, causing recurring swelling and shrinkage that can lead to sudden landslides (John, 2020).

High rainfall in East Malaysia, particularly in the Sabah region, increases the risk of landslides by saturating the soil and rock, especially in areas with residual soils, shale, and sandstone. This saturation disrupts soil cohesion and enhances the likelihood of slope failure (Roslee, 2018; Rosly et al., 2022). Furthermore, the development in Sandakan over the past decades has intensified these risks, with land clearing and urbanization altering natural slopes and modifying drainage patterns (Roslee, 2018).

Although significant research has been conducted on the behaviour of unsaturated soils in Sabah, the specific impact of rainfall on the stability of the Garinono Formation has not been thoroughly investigated. This study aims to address this gap by analysing the stability of unsaturated soils from the Garinono Formation during the rainy season. Using finite element methods and GEO-SLOPE International (2023) software, this research will simulate transient flow conditions to assess the soil's stability response. The findings will provide valuable insights into the hydro-mechanical behaviours of the Garinono Formation, which are crucial for improving slope stability analysis and geotechnical design in the region.

3. Materials and Methods

3.1 Study Area and Data Collection

The study area, marked as location "P" in Figure 1, is situated within the Garinono Formation, which experiences regular mass movements contributing to slope instability (Musta et al., 2019). The study site is located at 5.7521 N, 117.7916 E, approximately 56.7 km from Sandakan town.

The study incorporates both field and laboratory data. Site Investigation (SI) work was conducted to gather detailed information on soil composition, stratigraphy, and shear strength. Fieldwork included drilling a borehole and collecting both disturbed and undisturbed soil samples. The disturbed samples were used to develop a comprehensive soil profile, while the undisturbed samples were analysed in the laboratory to assess the characteristics of the Garinono Formation soil. Additionally, ten years of rainfall data were obtained from the Department of Irrigation and Drainage (DID) Sabah to help identify patterns and critical thresholds related to slope instability.

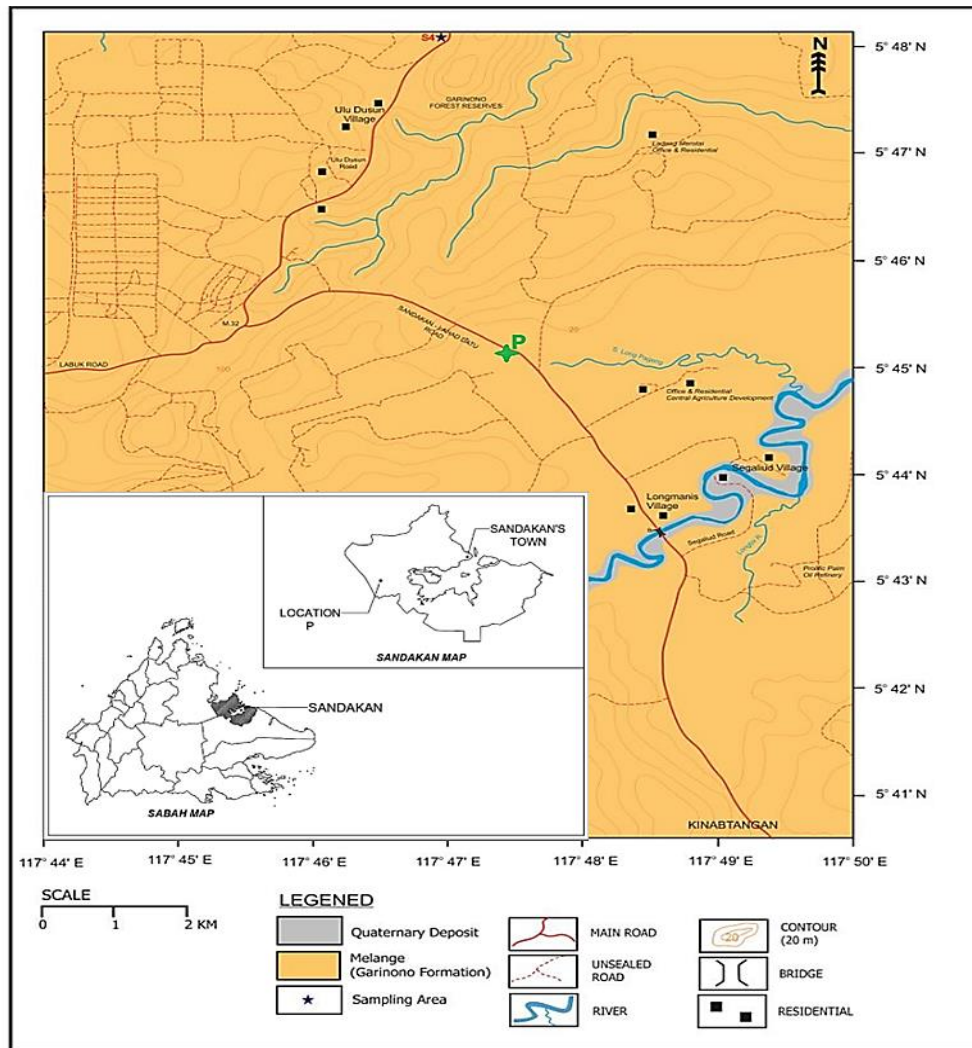


Figure 1 Geological map and study area location at the Garinono Formation Sandakan, Sabah. Source Musta et al., (2019).

3.2 Soil Physical Properties and Shear Strength Parameters

The importance of soil particle size and distribution is significant in geotechnical engineering. Studies suggest particle and grain size distribution affects soil properties. Knowing whether the soil is clay, sand, rock, gravel, or silt is insufficient in many engineering applications (Liu, & Evett, 2008). This research analysed disturbed soil samples for identification and classification. These samples were taken from boreholes to provide a baseline understanding of the physical properties of the soil. The classification tests included particle size distribution, Atterberg limits, and particularly specific gravity (SG), which reflects the mineral composition of the soil particles. The testing followed BS 1377:

Part 2 and the British Soil Classification System (The European Union, 1997).

Soil shear strength is crucial for slope stability analysis. According to Xi et al., (2021), the strength of unsaturated soil includes factors such as effective cohesion, intergranular friction, matric suction, and solute suction. Matric suction enhances soil shear strength, bearing capacity, and the slope stability safety factor (Sheng et al., 2009). In this study, triaxial strength tests were performed on undisturbed samples following standard procedures. The shear strength characteristics, including cohesion (c) and friction angle (ϕ), were determined using triaxial strength tests.

The shear strength characteristics, including total cohesion (c) and friction angle (ϕ), as well as effective

cohesion (c') and friction angle (ϕ'), were determined using the Consolidated Isotropic Undrained (CIU) triaxial test. In this test, soil samples are first consolidated under isotropic stress and then subjected to undrained loading, simulating short-term field conditions. The CIU test measures both pore water pressure and effective stress, allowing the assessment of total (c and ϕ) and effective (c' and ϕ') stress parameters. This test is particularly suitable for cohesive soils, considering both long-term consolidation and short-term undrained behaviour, ideal for slope stability analysis. The tests were done following the approach by Bishop, & Henkel (1962) and performed according to BS 1377 (1990).

The physical characteristics of the Garinono Formation soil (Table 1), derived from SI work, provide essential insights into the soil's composition, stratigraphy, and geotechnical properties. The investigation focused on two distinct layers: Layer (I), located at depths of 1.5 to 3.5 meters, and Layer (II), at 4.50 to 7.90 meters. Layer (I) is characterized by a higher clay content, with variations in plasticity and moisture content. The bulk and dry unit weights in this layer

reflect the influence of the clay and silt composition, with significant moisture content contributing to the lower dry unit weight. In contrast, Layer (II) is denser, with a slightly higher proportion of silt and gravel. This layer exhibits higher bulk and dry unit weights, which are indicative of a more compact and stiff soil structure.

In Table 2, the shear strength parameters reflect the distinct behaviour of Layer (I) and Layer (II) under varying conditions. Both layers exhibit similar cohesion under effective stress, 10.00 kPa, indicating comparable natural particle bonding. However, Layer (II), with more silt, sand, and gravel content, achieves a higher friction angle of 18.43° due to better particle interlocking, enhancing its resistance to shear deformation in drained, long-term conditions. Conversely, Layer (I), with higher clay content, shows greater cohesion of 16.00 kPa under total stress, driven by suction effects, which provides better stability during rapid, undrained loading. These parameters align with geotechnical principles and reflect the natural heterogeneity of the Garinono Formation, ensuring reliable inputs for slope stability modelling.

Table 1 Summary of physical properties in the study area

| Sample Layer | Layer (I) | | | Layer (II) |
|--|--|-----------|-----------|--|
| Soil Description | Silty CLAY with weathered Shale fragments. | | | Silty CLAY with weathered Shale fragments. |
| Colour | Yellowish brown | | | Grey |
| Nature | Firm to stiff | | | Stiff to very stiff. |
| Sample Depth (m) | 1.5 – 2.0 | 2.0 – 2.5 | 3.0 – 3.5 | 4.50 – 7.90 |
| BS Classification | CI | ML | MI | ML |
| Particle Size Distribution (%) | | | | |
| Clay, 0.002 mm | 52 | 48 | 36 | 35 |
| Silt, 0.063 to 0.002 mm | 40 | 49 | 48 | 51 |
| Sand, 2 to 0.063 mm | 6 | 2 | 6 | 6 |
| Gravel, 63 to 2 mm | 2 | 1 | 10 | 8 |
| Atterberg Limit (%) | | | | |
| Liquid Limit (L.L) | 39 | 34 | 36 | 34 |
| Plastic Limit (P.L) | 16 | 22 | 15 | 22 |
| Plastic Index (P.I) | 23 | 12 | 21 | 12 |
| Natural Moisture Content (%) | 39.45 | 10.76 | 27.84 | 12.94 |
| Specific Gravity (SG) | 2.476 | 2.433 | 2.688 | 2.60 |
| Bulk Unit Weight γ_b (kN/m ³) | 19.32 | 18.51 | 18.17 | 21.71 |
| Dry Unit Weight γ_d (kN/m ³) | 13.85 | 16.72 | 14.21 | 19.22 |

Table 2 Shear strength parameters of Garinono Formation used in numerical simulation

| Shear Strength | Layer (I) | Layer (II) |
|-----------------------------|-----------|------------|
| Sample Depth (m) | 1.5 – 3.5 | 4.5 – 7.9 |
| Effective Stress | | |
| Cohesion, c' (kPa) | 10.00 | 10.00 |
| Friction Angle, ϕ' (°) | 17.57 | 18.43 |
| Total Stress | | |
| Cohesion, c (kPa) | 16.00 | 12.00 |
| Friction Angle, ϕ (°) | 12.72 | 14.57 |

3.3 Hydraulic Properties of the Garinono Formation

Undisturbed samples, taken at a depth of 1.5 meters below the ground level, were used to measure bulk density (ρ_b) and obtain the Soil Water Characteristic Curve (SWCC) parameters. These samples retained their natural structure, porosity, and moisture content, which are essential for accurately modelling soil-water retention behaviour. Volumetric water content and bulk density were measured using a pressure plate extractor, ensuring reliable results across a range of soil types, from coarse to fine-grained, and covering suction pressures between 1 and 1500 kPa (Azmi et al., 2019; Sharratt, 1990).

The pressure plate extractor was tested under ASTM (2000). The equipment had a burette to measure extracted water and a high-pressure chamber. Soil samples were placed in fifteen rings, each with an inner diameter of 0.045 m and a height of 0.05 m, across five large-capacity pressure plate moisture extractors (Soil Corp.® pressure plates, ranging from 1 to 15 bar pressures). Sample rings rested on saturated cellulose membranes. Water was drained from the membrane through a constricted opening at the bottom. All pressure plate moisture extractors were set overnight.

The specimens were weighed for dry mass and gravimetric water content. Equation (1) was used to compute soil sample volumetric water content (θ). SWCC then linked volumetric water content to matric suction.

Volumetric Water Content:

$$\theta = \frac{w}{100} \times \rho_b \quad (1)$$

Where, w is Gravimetric Water Content:

$$w = \frac{W_a - W_b}{W_b} \times 100 \% \quad (2)$$

Where, W_a is the weight of the moisture sample, W_b is the weight of the dried sample.

The undisturbed sample tube, measuring 30 cm in length, was used to gather four samples in the study area. Samples were collected from two distinct layers in the slope profile. From Layer (I), at a depth of 1.5 to 3.5 meters, three samples were taken: (i) MI, (ii) ML, and (iii) CI. An additional sample was collected from Layer (II), at a depth of 4.5 to 7.9 meters, classified as ML. The Soil-Water Characteristic Curve (SWCC) for all samples and bulk densities obtained from both layers was tested using a pressure plate extractor. The volumetric water content versus soil suction test was employed in this study, as it was recognized to be a straightforward method for

measuring unsaturated soil relationships by Fredlund, & Fredlund (2020).

In addition, previous researchers have indicated that empirical models can effectively capture the variation in water content with changing soil suction. This study adopted an empirical model, as it has been found to predict soil suction-induced water content variations. Leong, & Rahardjo (1997b) discovered that soil type, mineral concentration, and pore architecture affect model success. Cornelis et al., (2005) found that clay percentage improves model performance and decreases as sand content increases. Yamusa et al., (2019) conclude that Fredlund, & Xing's (1994) (FX) models fit most soil water retention curves. In addition, Leong, & Rahardjo (1997a) suggested that the FX equation can be used for a wide range of soils over the entire range of matric suction. Therefore, the Fredlund, & Xing (1994) empirical model was selected to depict the SWCC behaviours of the Garinono Formation, and it was concluded by Nassor et al., (2024) to be the most suitable model for representing the soil's SWCC, covering the full range of suction from low to high values. Equation (3) shows the Fredlund, & Xing (1994) used.

Volumetric water content:

$$\theta = \theta_r + \frac{\theta_s - \theta_r}{\{\ln[e + (\psi/a)^n]\}^m} \quad (3)$$

Where, θ_s is saturated volumetric water content ($cm^{-3} cm^{-3}$), is θ_r residual volumetric water content ($cm^{-3} cm^{-3}$), ψ is matric suction (kPa), e is the Euler number, an irrational constant equal to 2.71828 in natural logarithm, a is a parameter closely related to the air-entry value, but the value is higher than the air-entry value (kPa). At the same time, n and m are the slopes at the inflexion point of the SWCC.

To improve the SWCC model and parameters, we used statistical analysis scores like R-Square (R^2) and root mean square error (RMSE) in the Excel solver software tool. The values of R^2 indicate the model's fit to the experimental and fitted data sets (Habasimbi, & Nishimura, 2019). On the other hand, the RMSE technique calculates the difference between the expected and actual values to evaluate the model's performance (Tao et al., 2020). Previous studies have consistently shown that R^2 values close to 1 provide accurate numerical representations of the results, while RMSE near zero optimises model performance (Harisuseno, & Cahya, 2020; Esmaeelnejad et al., 2015; Tao et al., 2020).

3.4 Permeability Functions for Unsaturated Soils

In this study, the saturated hydraulic conductivity, K_s was not directly measured in the laboratory but instead estimated using Equation (4), proposed by Zhai, & Rahardjo (2015) for saturated hydraulic conductivity. Equation (5) was used to calculate the air entry value (AEV) proposed by Zhai, & Rahardjo (2011). These equations are based on the FX model, while Equation (4) relies on the degree of saturation. It's worth noting that these model equations (4 and 5) are widely recognized and accepted within the academic community for predicting unsaturated values, as supported by various researchers, including Zhai et al. (2017). In addition, the soils' unsaturated behaviours were observed directly from the GEO-SLOPE International (2023) software.

Coefficient of Permeability:

$$K_s = \frac{1}{8} n^2 \left\{ \sum_{i=1}^N \left[[1-S(\psi_i)]^2 - [1-S(\psi_{i-1})]^2 \right] r_i^2 \right\} \quad (4)$$

Where, $S(\psi_i)$ and $S(\psi_{i-1})$ is degrees of saturation corresponding to soil suctions ψ_i and ψ_{i-1} respectively, N is the total number of the divided SWCC segments, and r_i is the radius of the capillary tube.

Air Entry Value (AEV):

$$\psi_{aev} = a * 0.1 \frac{3.72 * 1.31^{n+1} \left(1 - e^{-\frac{m}{3.67}} \right)}{n * m * \ln 10} \quad (5)$$

3.5 Rainfall Patterns and Landslide Correlation in Sandakan, Sabah

To understand the distribution of regional rainfall in the study area, an analysis was conducted on the rainfall patterns within Sandakan, Sabah, spanning a decade from 2010 to 2020. The data used for this study were sourced from the Sandakan Rain Gauge Station, provided by the Department of Irrigation and Drainage (DID) in Sabah. Additionally, a review of landslide events in Sandakan was carried out to identify critical periods when rainfall triggered landslides.

The State Environmental Conservation Department (ECD), Sabah (2001) report found that landslides and instability impair slope development, building site excavation, and road cuts, particularly in the Kundasang and Sandakan regions, where sedimentary rocks underlie the hilly topography of the west coast. Matlan et al., (2021) and Rosly et al., (2022) examined the relationship between rainfall and slope failure, indicating that many landslides in Ranau (an area near Sandakan) and Sabah occurred during the rainy seasons, with rainfall being the primary triggering factor. Table 3 presents the most prevalent times of landslip activity in Sandakan. It shows that landslides in the Sandakan region were commonly reported at the end of the Northwest Monsoon season, which is around December to February. Given the landslide history in Table 3, January has the highest slope failure rates. Therefore, this study focused on rainfall in January from 2010 to 2020 as a key factor in numerical modelling.

Table 3 Landslide history in the Sandakan region

| Date | Location | Source |
|-----------------|---|---|
| January - 1996 | Taman Foh, Sandakan, Sabah Jalan Penampang, Sandakan, Sabah | |
| February - 1996 | Taman Nam Tung, Sandakan, Sabah | (Malaysia Kementerian Kerja Raya |
| January - 1999 | Squatters Settlement, Sandakan, Sabah | Jabatan Kerja Raya, 2009) |
| February - 1999 | Jalan Leila, Kg. Gelam, Sandakan, Sabah | |
| February - 2006 | Kampung Sundang Darat, Batu Sapi, Sandakan, Sabah | |
| December - 2006 | Sandakan roads hit by landslip, flash floods; Mudslide destroys two houses in Sandakan; Landslide on Agnes Keith Road, Sandakan | Natural Disaster Research Centre (NDRC), UMS (2023) |
| January - 2007 | Student Dies in Landslide in Sandakan | |
| January - 2011 | Residential area in Sandakan Region | Izumi et al., (2019) |
| February - 2014 | Kg. Sungai Tiram area, Libaran, Sandakan | John, (2020) |
| January - 2014 | Landslide at Taman Indah Jaya, Sandakan | Borneo Post Online (2014) |
| January - 2021 | Jalan Aman, Sandakan Cemetery | Bernamea (2021) |
| January - 2021 | Jalan Buli Sim Sim Road, Sandakan | Malay Mail (2021) |
| January - 2022 | Kg Segaliud, Muslim Cemetery Kg Berhala Darat (Sim-Sim), Kg Bokara and Jalan Panglima Adam, Sandakan | Bernamea (2022) |

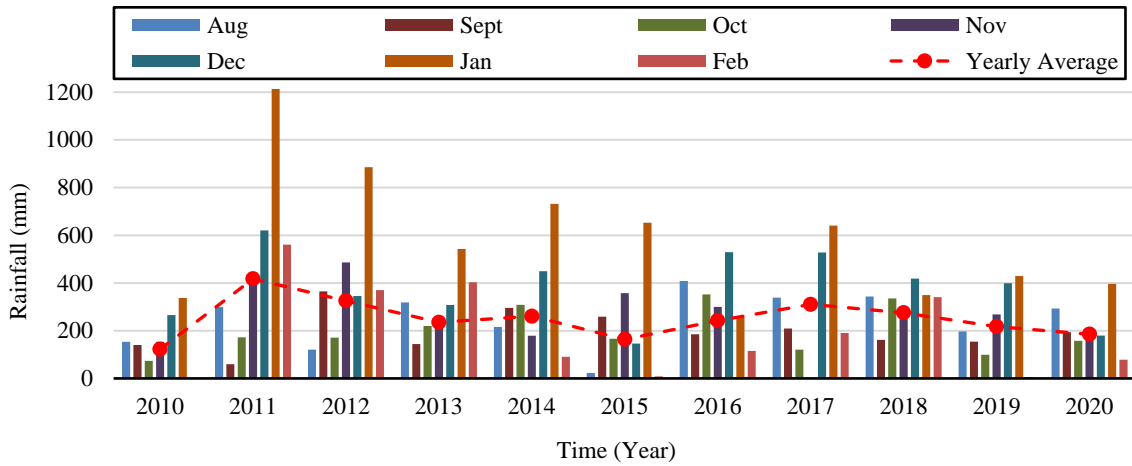


Figure 2 Distribution of monthly rainfall amount in Sandakan, Sabah from 2010 until 2020

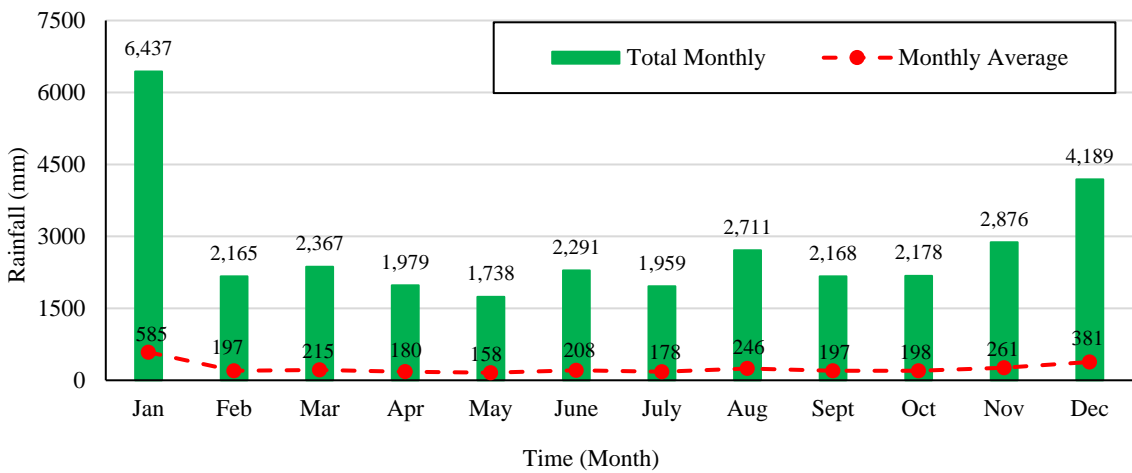


Figure 3 Total monthly rainfall and monthly average from 2010 to 2020 in the study area

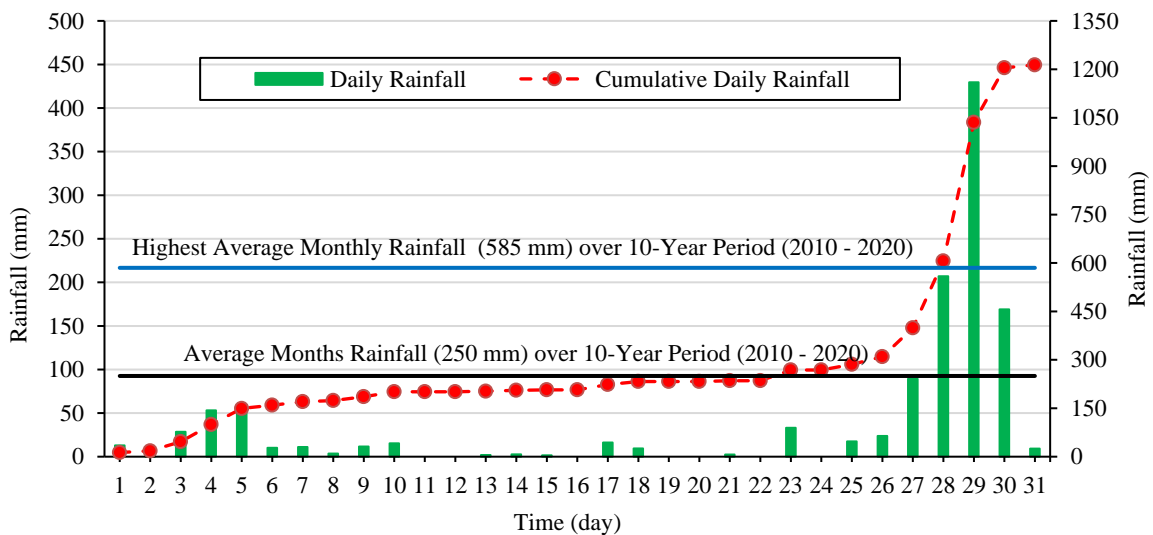


Figure 4 Daily rainfall distribution for the highest month recorded (2010–2020) in the study area

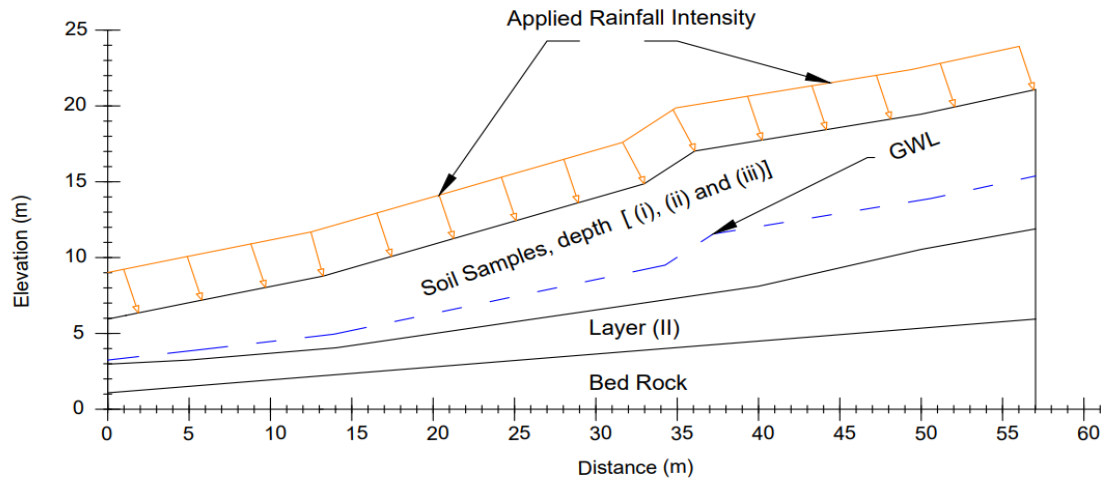


Figure 5 Original geometry of the soil profile in the study area

Figures 2 and 3 further illustrate that January experienced the highest monthly rainfall each year, with 2011 showing the highest annual average rainfall over the ten-year period from 2010 to 2020. These observations suggest that the peak of the rainy season in January is a triggering factor for slope instability in the study area.

Figure 4 shows the distribution of daily rainfall in January 2011, consisting of 31 days, during which the highest total monthly rainfall intensity was recorded in the study area. This month experienced unusually heavy rainfall, significantly exceeding the average monthly rainfall, with a total monthly rainfall of 1,213.90 mm. This data was used in the simulation to analyse the impact of severe hydrological conditions on slope stability.

3.6 Slope Geometry and Ground Condition

The slope geometry and groundwater levels (GWL) were determined during the site visit and investigation. On October 10, 2017, at 3:00 p.m., the GWL was approximately 0.10 meters below the ground surface. Three days later, the GWL was recorded at 0.50 meters, and five days after that, it was observed to have reached a depth of 5.70 meters from the surface. This significant variation in GWL, ranging from 0.10 meters to 5.70 meters, highlights the highly variable and partially unsaturated nature of the Garinono Formation. These fluctuations are likely influenced by factors such as precipitation, evaporation, and subsurface geological conditions. Understanding these variations is crucial for assessing slope stability, as changes in groundwater levels can

significantly affect the geotechnical behaviour of the slope.

Figure 5 illustrates the three-soil profile layers used in the numerical simulation, derived from site exploration data. These layers include Samples in Layer (I) (i.e., (i), (ii), and (iii)), Layer (II), and Bedrock. The slope spans a length of 57.03 meters and a height of 21.09 meters. Using a GWL of 5.70 meters in the simulation allows for a comprehensive analysis of slope stability under extreme hydrological conditions. This setup captures the interactions between soil moisture, pore-water pressure, and slope stability, providing a realistic assessment of potential failure mechanisms under an extremely rainfall scenario and groundwater fluctuations.

3.7 Slope Modelling and Parameters

The numerical simulation was conducted using GeoStudio software, specifically employing the Slope/W and Seep/W modules, with the Morgenstern-Price method to determine slope stability under both rainfall and non-rainfall conditions. In Seep/W, transient analysis was used to evaluate the process of rainfall infiltration into the slope. Figure 5 outlines the boundary conditions for rainfall input during January 2011, a period chosen for its highest rainfall levels, based on historical data from 2010-2020. This simulation represents an extreme rain pattern that has been linked to slope failures in the study area (see Table 3).

For numerical simulation, we utilised the slope configuration from Figure 5 and the groundwater table data from the Site Investigation report. While the analysis focuses on simulating the slope's behaviour

during heavy rainfall in January, the GWL data from October was selected to reflect the most recent and reliable site condition. The GWL at 5.70 m depth was chosen to ensure both saturated and unsaturated conditions were adequately represented in the simulation. The worst-case rainfall scenario in this analysis comes from the heavy rainfall event in January 2011. Using the GWL data from October, the model can simulate how rainfall affects slope stability under typical unsaturated conditions, providing for a more accurate assessment of the impact of rainfall infiltration on the slope during the extreme weather event.

Three regions were drawn on the slope, as shown in Figure 5; the first region was used for soil sample materials, sample (i), (ii), and (iii). The second and third regions were assigned to Layer (II) and Bed Rock, respectively and remained constant throughout the analysis of each soil sample.

Moreover, Figure 6 shows the mesh results from the GeoStudio software. The 2D elements geometry, including quadrilateral shapes with a one meter (1 m) element size, was used. Regarding boundary conditions, the rainfall intensity of 31 days was applied on the slope's surface. In addition, water heads on the left and right were set constant at 3.2 m (i.e., 2.16 m from the bedrock) and 15.83 m (i.e., 9.88 m from the bedrock) from the origin, respectively. A no-flow boundary was applied along the left and right boundaries above the groundwater table.

The study further examined the effects of rainwater infiltration on three different slope models for each soil sample in Layer (I) (i.e., samples (i), (ii), and (iii)) separately. The simulation considered factors such as saturated and unsaturated permeability, which affect the soil's water storage capacity and resulting pore-water pressure, to evaluate their impact on slope stability.

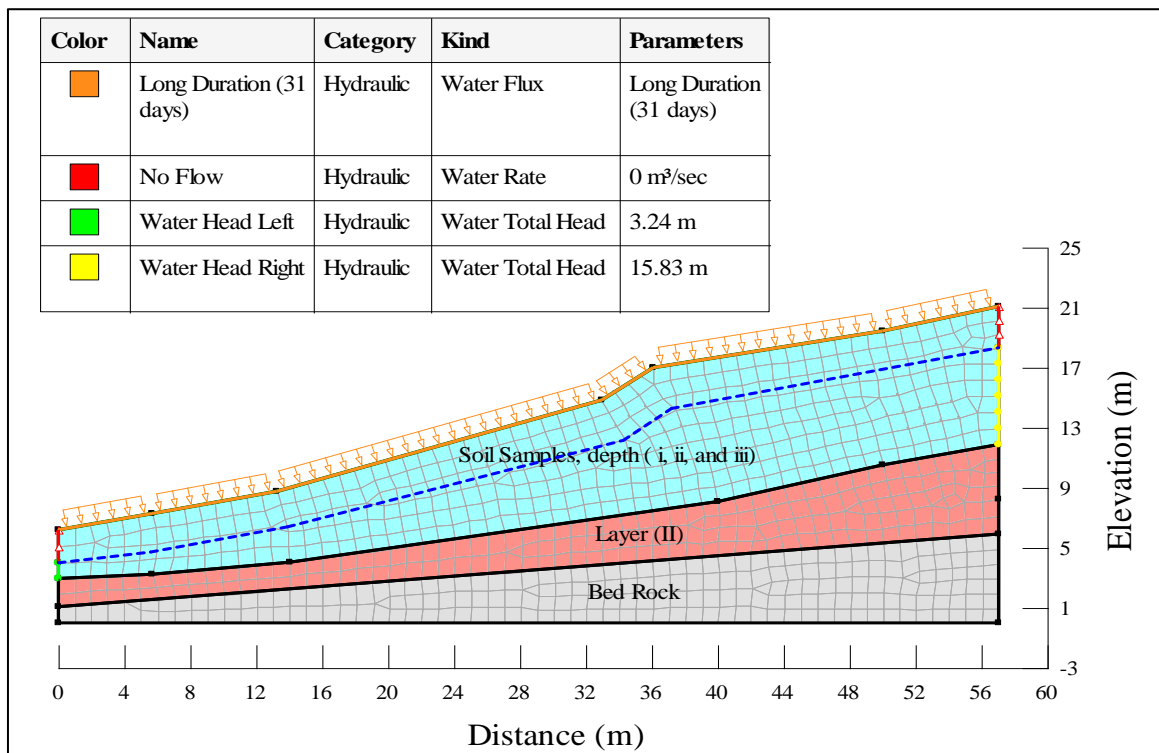


Figure 6 Boundaries conditions and mesh results of the slope profile

4. Results and Discussion

4.1 Soil Hydraulic Properties of Garinono Formation

The bulk densities (BD or ρ_b) of the Garinono soil samples are presented in Table 5. Bulk density typically reflects soil properties such as infiltration, water-holding capacity, and porosity. Moreover, soil hydraulics are influenced by the size and arrangement of pores, which are determined by the soil's bulk density (Prasad, & Pietrzykowski, 2020). The bulk densities of the undisturbed soil samples and layers correspond to the natural composition and characteristics of the soil formation in the study area. Sample (i) (MI) has a bulk density of 1.64 g/cm³, indicating a moderately plastic clay with a balanced mix of clay and silt, which is typical of soils with moderate moisture retention and compaction. Sample (ii) (ML), with the lowest bulk density of 1.48 g/cm³, represents low plasticity silt, resulting in a looser structure with less moisture retention. Sample (iii) (CI) has a bulk density of 1.94 g/cm³, reflecting a higher clay content that leads to greater moisture retention and a more compact, cohesive structure. Layer (II) exhibits the highest bulk density at 1.99 g/cm³, due to its higher silt and gravel content, which naturally results in a denser and stiffer soil structure.

Figure 7 depicts the SWCC of the soil samples (i), (ii), (iii) for Layer (I), and Layer (II), along with both the measured and fitted models. Table 5 highlights the R² values achieved by the FX model, which range from 0.9875 to 0.9935. Conversely, the model exhibited the lowest RMSE of 0.0006, while the highest RMSE value recorded was 0.0062. In summary, the FX model performed exceptionally well in representing the SWCC of Garinono soil using the available measured data in terms of RMSE and R² values. Furthermore, the FX model is the most suitable choice for Silt Clay in the Garinono Formation soil (Nassor et al., 2024). The FX

model covers the entire suction range (Figure 7), as indicated by the SWCC parameters, and predicts lower residual water content values, as shown in Table 4.

Based on the SWCC presented in Figure 7, it is evident that silty clay samples exhibit remarkable water retention capacity due to the unsaturated behaviour of the Garinono Formation, as similarly observed by Oluyemi-Ayibiowu et al., (2020) for the tropical clay soils. The soil samples exhibited a higher suction need, exceeding 1500 kPa, to extract all water from the sample due to the higher residual volumetric water contents (θ_r) of the measured data. This is because silty clay particles are smaller and finer when compared to sand particles. Silty clay retains water due to its finer particles, providing a larger surface area for bonding water molecules (Lu, & Godt, 2013). Furthermore, its dense structure enhances water retention by reducing the number of pores that allow water to drain or percolate (Zhao et al., 2022).

Table 5 shows soil Air Entry Value (AEV) and saturated hydraulic conductivity K_s of the samples. The hydraulic conductivity function behaviour of the soil samples shown in Figure 8 was presented using the FX model, obtained by employing the saturated hydraulic conductivity (K_s), and SWCC parameters in the GeoStudio software. The results show that sample (ii) has the highest saturated and unsaturated hydraulic conductivity, with K_s values of 5.3998E-08 m/sec. Next is the sample (i), which has K_s values of 2.4276E-08 m/sec, and the lowest values of K_s are the sample (iii) and layer (II), which has K_s value equal to 2.5788E-09 m/sec and 7.3498E-11 m/sec respectively. All Garinono Formation samples generally have lower saturated permeability relative to impermeable values; studies have confirmed that the presence of higher clay content causes lower hydraulic conductivity in soils (Das, & Sivakugan, 2019; White, 2018; Fell et al., 2005; Look, 2014).

Table 4 SWCC parameters and fitting performance for soil samples from the Garinono Formation

| Sample | Soil Type | Fredlund, & Xing (1994) | | | | | Fitting Values | | |
|------------|-----------|-------------------------|------------|------------|----------|--------|----------------|----------------|--------|
| | | ρ_b | θ_s | θ_r | a | n | m | R ² | RMSE |
| (i) | MI | 1.64 | 0.3402 | 0.0005 | 20.109 | 1.0572 | 0.1343 | 0.9906 | 0.0022 |
| (ii) | ML | 1.48 | 0.2780 | 0.1366 | 13.554 | 1.6032 | 0.1577 | 0.9983 | 0.0006 |
| (iii) | CI | 1.94 | 0.3061 | 1.78E-10 | 151.150 | 0.8379 | 0.2082 | 0.9875 | 0.0062 |
| Layer (II) | ML | 1.99 | 0.3810 | 0.1449 | 571.1880 | 0.4494 | 0.4845 | 0.9935 | 0.0010 |

Table 5 AEV and saturated hydraulic conductivity K_s , values for the soil samples

| Sample | ψ_{aev} (kPa) | K_s (m/s) |
|------------|--------------------|-------------|
| (i) | 3.90 | 2.4276E-08 |
| (ii) | 3.88 | 5.3998E-08 |
| (iii) | 21.90 | 2.5788E-09 |
| Layer (II) | 25.10 | 7.3498E-11 |

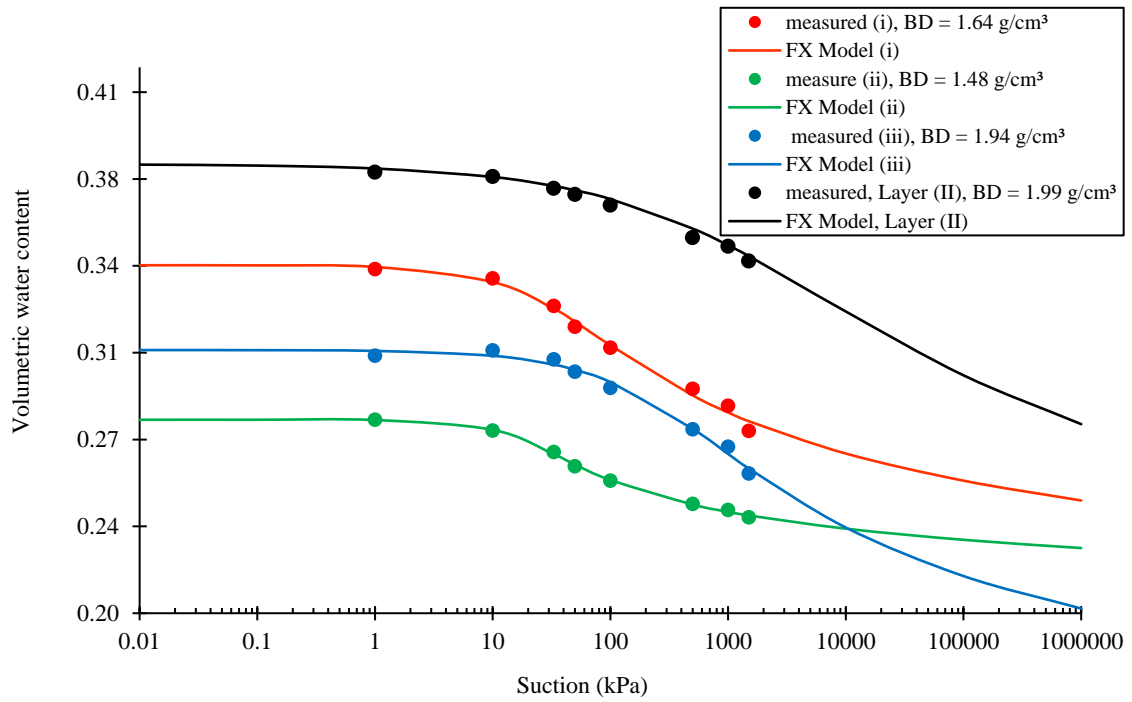


Figure 7 SWCC of the soil samples (Based on FX model values)

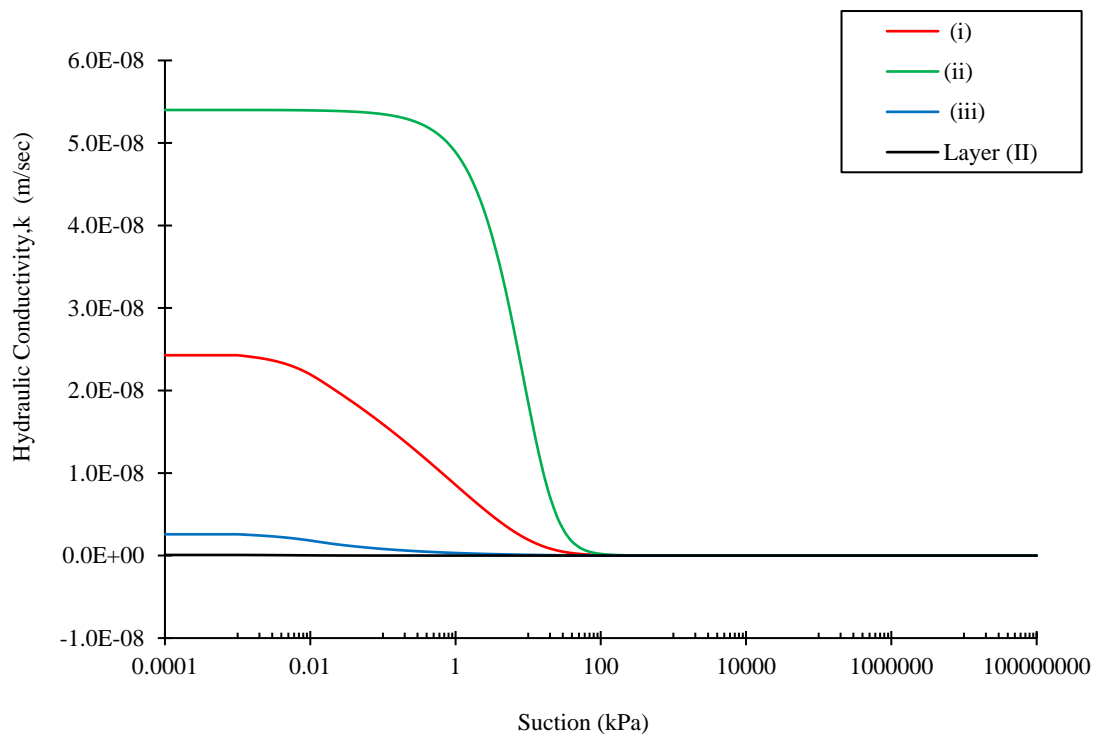


Figure 8 Hydraulic conductivity function of the different soil samples

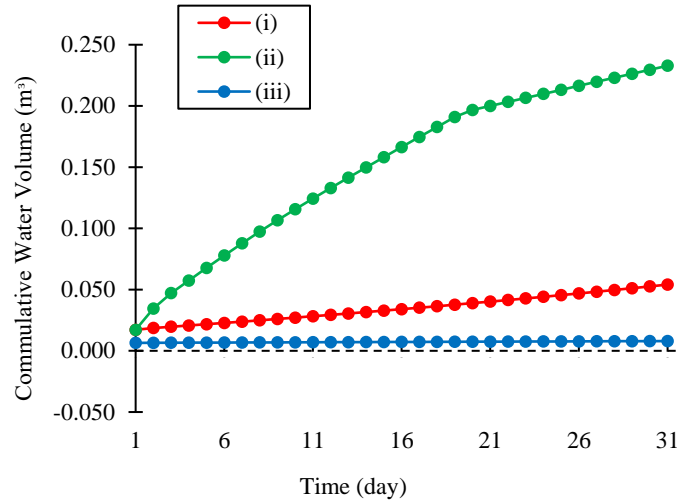


Figure 9 Cumulative water volume of the samples during 31 days of rainfall events

4.2 Numerical Simulation and Results

4.2.1 Cumulative Water Volume (m^3)

Figure 9 illustrates the cumulative volume of water (m^3) present in the soil mass following a rainfall event on soil samples. The findings reveal that this cumulative volume increases as the intensity of the rainfall event rises. The soils can retain a certain amount of water, which varies based on soil type and the rainfall pattern.

The figure highlights the important roles of saturated conductivity (K_s) and unsaturated conductivity ($K(\theta)$) in influencing soil infiltration and cumulative water volume within the soil cross-section after rainfall. Samples with higher K_s and $K(\theta)$ values show greater water retention, as seen in Table 5 and Figure 8. For example, sample (ii) has the highest cumulative water volume due to its K_s value of $5.3998E-08$ m/sec, while sample (iii) has the lowest cumulative volume, corresponding to its lower K_s value of $2.5788E-09$ m/sec. Sample (i) falls between the two, with a K_s value of $2.4276E-08$ m/sec.

The FX fitting parameter n , which signifies the rate of water extraction from the soil, also plays a crucial role in water storage (Abhisekh et al., 2016; Song et al., 2015). Figure 9 shows that sample (ii) has the highest cumulative water volume, driven by its higher n value of 1.6032, followed by sample (i) with an n value of 1.0572. Sample (iii) shows the lowest cumulative water volume due to its lower n value of 0.8379. Although sample (ii) has a slightly higher K_s value than sample (i), its higher cumulative water volume is primarily due to its larger n value.

Similarly, sample (iii) has a low cumulative water volume results from both its lower K_s and n values.

In summary, ML soils, represented by sample (ii), exhibit the highest cumulative water volume after rainfall due to their higher hydraulic conductivity (K_s) and extraction rate (n). MI soils (sample i) show moderate water volumes, while CI soils (sample iii) have the lowest cumulative water volumes.

4.2.2 Effect of ratio on rainfall intensity, $q(I)$ to soil saturated permeability (i.e., $(q(I)/K_s)$) on Discharge

The relationship between rainfall intensity and soil-saturated permeability is crucial for monitoring the responses of suction and groundwater table fluctuations during rainfall infiltration in a soil slope. In this study, it was observed that the q/K_s ratio exhibited remarkably high values, primarily attributable to the notably low saturated permeability of the Garinono Formation soil. This phenomenon aligns with the findings of Yang, & Huang (2023), who noted that soil's lower saturated hydraulic conductivity can lead to a substantial portion of the rainfall on the slope being transformed into surface runoff. Consequently, this minimizes the influence of rainfall on the infiltration behaviour.

As depicted in Figure 10, sample (iii) exhibited the highest q/K_s ratio due to its remarkably low saturated permeability ($K_s = 2.5788E-09$ m/sec), leading to significant runoff and reduced infiltration within the slope matrix. This resulted in the lowest cumulative water storage and slightly higher water discharge rates, as indicated in Figures 9 and 11. In

contrast, samples (i) and (ii), with higher K_s values (2.4276E-08 m/sec and 5.3998E-08 m/sec, respectively), exhibited lower q/K_s ratios, contributing to less surface runoff, higher cumulative water storage, and reduced discharge rates. Figures 10 and 11 illustrate that the CI soil type (sample iii) generated more runoff, while the MI (sample i) and ML (sample ii) soils experienced moderate to high infiltration and minimal discharge, respectively.

4.2.3 Matric Suction (kPa)

Figure 12 depicts changes in suction over 31 days of rainfall events along the slip surface, from 13.0 m to 49.0 m horizontally from the origin. The data reveal a decrease in matric suctions as rainfall intensifies, consistent with previous studies (Rehan et al., 2024; Rosly et al., 2022; Ng & Shi, 1998). However, this study highlights variations in suction reduction among soil samples, ranging from 17.30%

for sample (iii) to 59.92% for sample (i), with complete reductions of 100% for sample (ii).

Sample (iii), which exhibited the smallest suction reduction (17.30%), also had the lowest cumulative water volume (Figure 9) and a higher discharge rate (Figure 11), due to its higher q/K_s ratio (Figure 10). In contrast, samples (i) and (ii), with greater suction reductions of 59.92% and 100%, respectively, showed higher cumulative water volumes and lower discharge rates, corresponding to their lower q/K_s ratios.

Overall, Figure 12 illustrates that CI soil (sample iii) experienced the smallest decrease in matric suction, maintaining the highest suction levels due to lower water infiltration. MI soils (sample i) showed moderate suction reductions, while ML soils (sample ii) experienced the largest decrease, resulting in the lowest suction values.

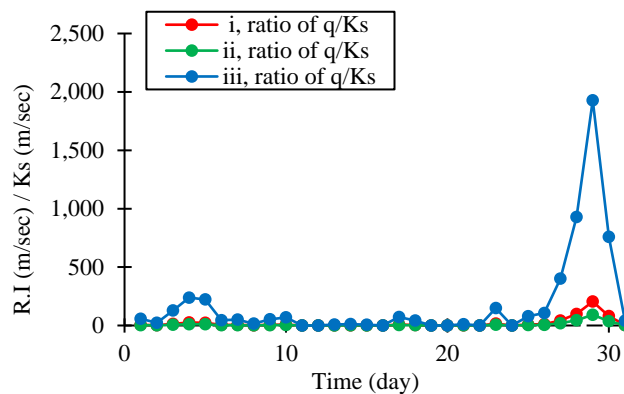


Figure 10 Ratio of rainfall intensity to the saturated hydraulic conductivity of the samples (for 31 days of rainfall events)

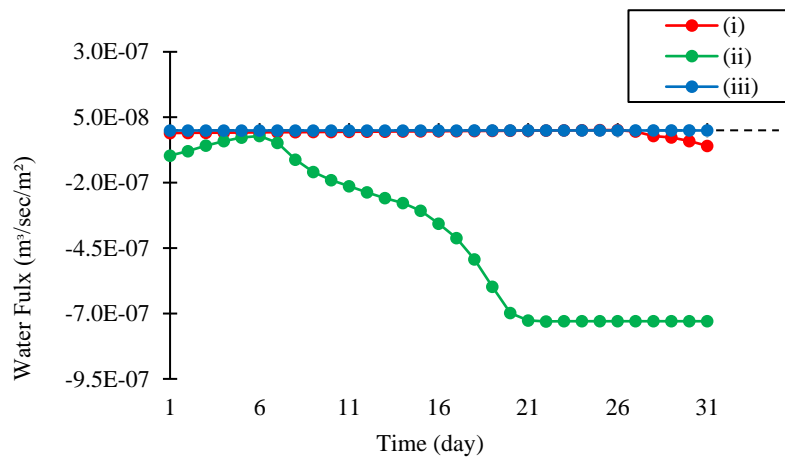


Figure 11 Discharge rate of the samples during 31 days of rainfall events

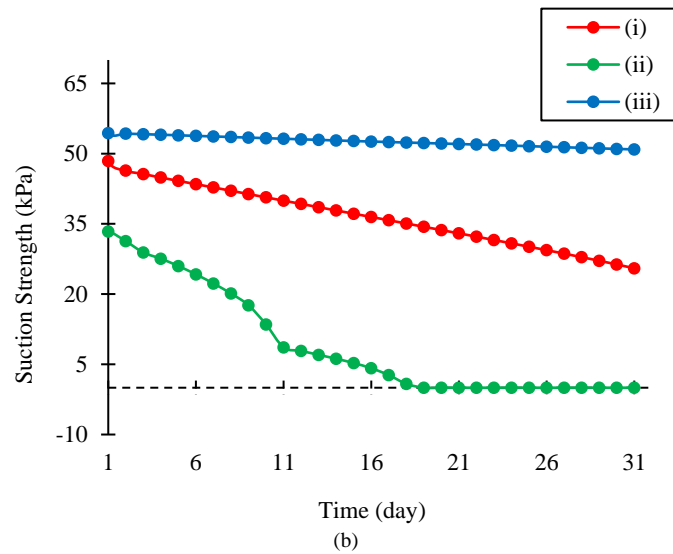


Figure 12 Suction variation of the samples during 31 days of rainfall events

4.2.4 Pore-Water Pressure (PWP) Development

Figures 13(a) and (b) illustrate the evolution of pore water pressure within the soil mass during rainfall events. Various factors contribute to PWP development, including vegetation cover (Ng et al., 2015), soil type (Liu et al., 2021), rainfall intensity (Yunusa et al., 2014), rise in groundwater level (Oluyemi-Ayibiowu et al., 2020), the presence of a crack in the soil mass (Cao et al., 2016). Pore-water pressure in soil or rock acts within particles or pores and serves as a crucial indicator of soil stress changes. The analysis highlights notable PWP differences among the samples. Additionally, PWP rises with rainfall, as observed by previous studies (Xue et al., 2016; Yuan et al., 2020), due to the dissipation of matric suctions in the slope, leading to larger pore water pressure with higher suction reduction.

Figure 13(a) shows that sample (ii) exhibits earlier and higher increases in PWP compared to the other samples, which can be attributed to its higher suction reductions (Figure 12) and higher cumulative water content (Figure 9). Conversely, samples (iii) and (i) display high negative PWP values due to their

lower suction reductions and lower cumulative water content during the 31-day rainfall event.

Furthermore, Figure 13(b) indicates that samples (iii) and (i) show higher negative PWP values on the slope surface, suggesting that these samples remained more unsaturated compared to sample (ii). This is due to their lower cumulative water volumes, preventing full saturation, as seen in Figure 9. This behaviour aligns with findings from previous studies (Yuan et al., 2020; Fathiyah, & Bahsan, 2016), which also observed a gradual increase in PWP during rainfall. Conversely, sample (ii) shows higher positive PWP values, indicating full saturation due to its higher cumulative water volume.

Overall, Figures 13(a) and 13(b) highlight the variations in PWP among the three soil samples after 31 days of rainfall, underscoring the importance of matric suction in slope stability. CI soil, represented by sample (iii), maintains the lowest and most negative PWP values, corresponding to its highest suction levels. MI soil (sample i) displays moderate PWP values, while ML soil (sample ii) experiences significant suction reductions, resulting in the highest PWP values.

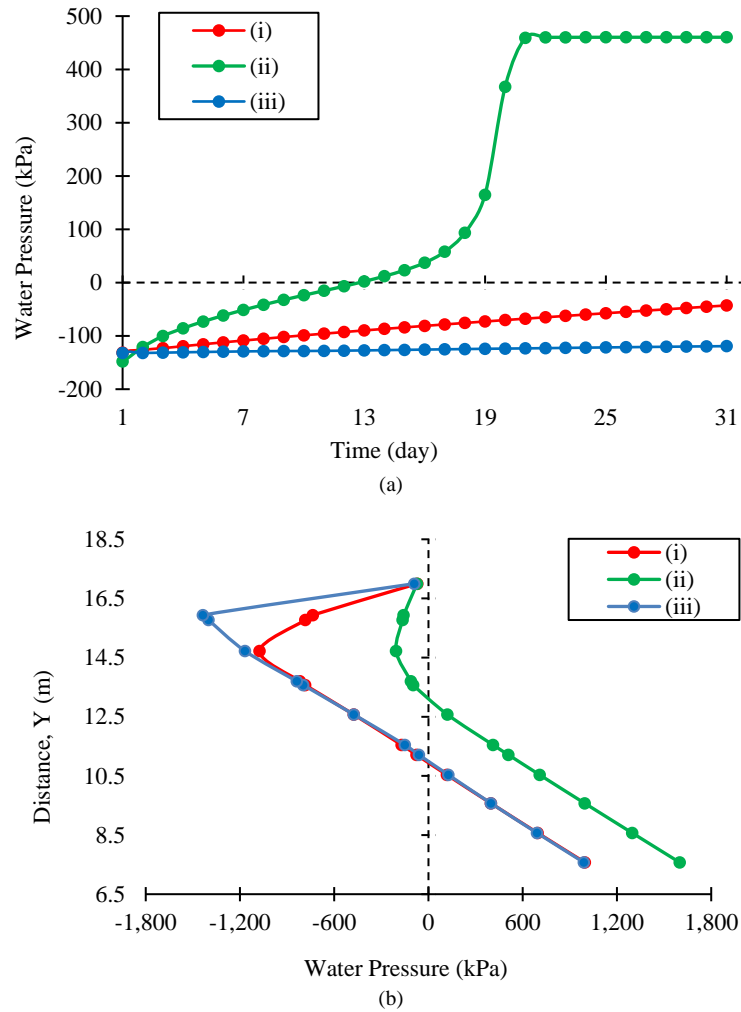


Figure 13 Pore-water pressure of the samples during 31 days of rainfall event:(a) PWP development; (b) PWP profile

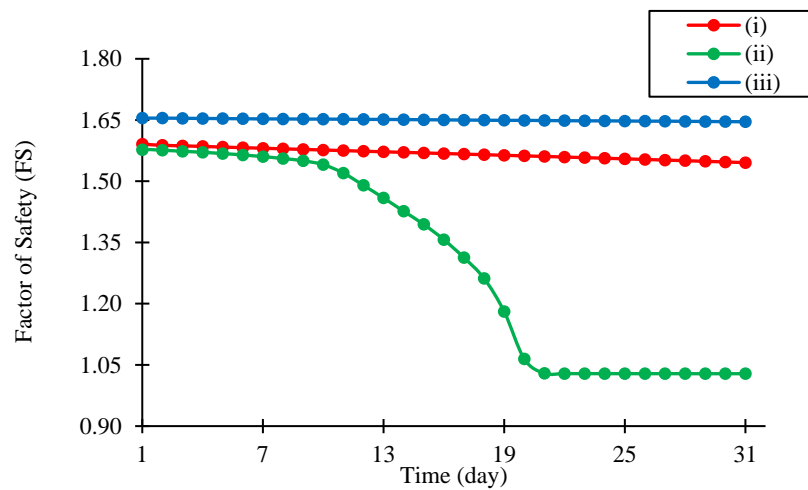


Figure 14 Factor of safety (FS) variation of the samples during 31 days of rainfall events

4.2.5 Factor of Safety (FS)

Figure 14 shows the Factor of Safety (FS) during a 31-day rainfall simulation, highlighting the decreasing stability of Garinono soil under rainfall, with variations in FS depending on soil type.

Sample (ii) exhibited the lowest FS values during the rainfall event, followed by sample (i), whereas sample (iii) demonstrated the highest FS values. The higher FS in sample (iii) was due to a lower cumulative water volume within the slope (Figure 9) and higher water discharge (Figure 11), attributed to its higher q/K_s ratio (Figure 10). This led to higher suction values (Figure 12) and reduced pore water pressure (PWP), ultimately enhancing slope stability, consistent with findings from Fathiyah, & Bahsan, (2016) and (Rahardjo et al. (2012), where negative PWP contributed to increased shear strength, making slopes less prone to failure. Moreover, the results align with Yang et al. (2019) findings, indicating that soils with lower permeability experience minimal suction decreases, enhancing stability. Similarly, Fan, & Zeng (2016) concluded that lower K_s values lead to minimal safety factor changes during rainfall.

In contrast, sample (ii) had the lowest FS values, primarily due to its lower q/K_s ratio and higher K_s value (see Figure 10), which resulted in increased infiltration and reduced surface runoff. Consequently, sample (ii) accumulated more water during rainfall events (Figure 9), leading to lower suction (Figure 12) and the highest PWP (Figure 13), reducing slope stability. Sample (i) showed intermediate FS values due to its moderate q/K_s ratio and K_s , cumulative water volume, suction, and PWP compared to the other samples. The decrease in FS for sample (i) was largely due to increased PWP, which reduced shear strength and heightened the potential for slope failure (Yang, & Huang, 2023; Ng, & Shi, 1998; Xue et al., 2016). This rise in PWP was caused by the dissipation of matric suction as cumulative water volume increased during rainfall, leading to higher soil water content and decreased effective stress (Pan et al., 2020).

In summary, Figure 14 illustrates the variation in slope stability for the three soil samples. CI soil (sample iii) exhibited the highest stability due to gradual PWP increases and greater suction retention, linked to lower cumulative water volume. MI soils (sample i) showed moderate stability, while ML soils (sample ii) had the lowest stability due to higher cumulative water content, rapid saturation, greater

suction reduction, and higher positive PWP values during rainfall.

5. Conclusion

This study provides valuable insights into the hydraulic behavior and stability of Garinono Formation soils during rainfall events. Key findings include the significant influence of rainfall intensity and soil permeability on slope hydrology and stability, the crucial role of the q/K_s ratio in determining infiltration and runoff patterns, and the varying impacts of rainfall on different soil types, with ML soils showing the highest vulnerability to failure, while MI soils demonstrating moderate stability and CI soils maintaining better stability. The Garinono Formation's silty clay soils are prone to reduced suction and increased pore pressure during rainfall, highlighting the importance of these factors in slope stability assessments. While these findings have important implications for construction projects in rainfall-prone regions, the study's specificity to the Garinono Formation and assumptions of soil homogeneity limit its generalizability. Further research is recommended to explore long-term rainfall impacts, varying initial conditions, and the effects of surface runoff and subsurface erosion on soil stability, which will be crucial for improving safety and design effectiveness in similar geological contexts.

6. Acknowledgments

The authors gratefully acknowledge the financial support from Universiti Malaysia Sabah through the GUG0577-1/2023 and GUG0384-2/2019 grants, as well as the Ministry of Higher Education Malaysia through the RACER29-2019 grant.

7. References

- Abhisekh, S., Yamsani, S. K., & Sreedeeep, S. (2016, December 15-17). *Effect of soil plasticity and presence of fine particles on SWCC* [Conference presentation]. Indian Geotechnical Conference IGC2016, Chennai, India.
- ASTM, D. (2000). Standard Test Method for Capillary-Moisture Relationships for Coarse- and Medium- Textured Soils by Porous-Plate Apparatus. *Annual Book of ASTM Standards, 04*(Reapproved), 1–6.
- Azmi, M., Ramli, M. H., Hezmi, M. A., Mohd Yusoff, S. A. N., & Alel, M. N. A. (2019, May 18-22). Estimation of Soil Water Characteristic Curves (SWCC) of mining sand using soil suction modelling [Conference

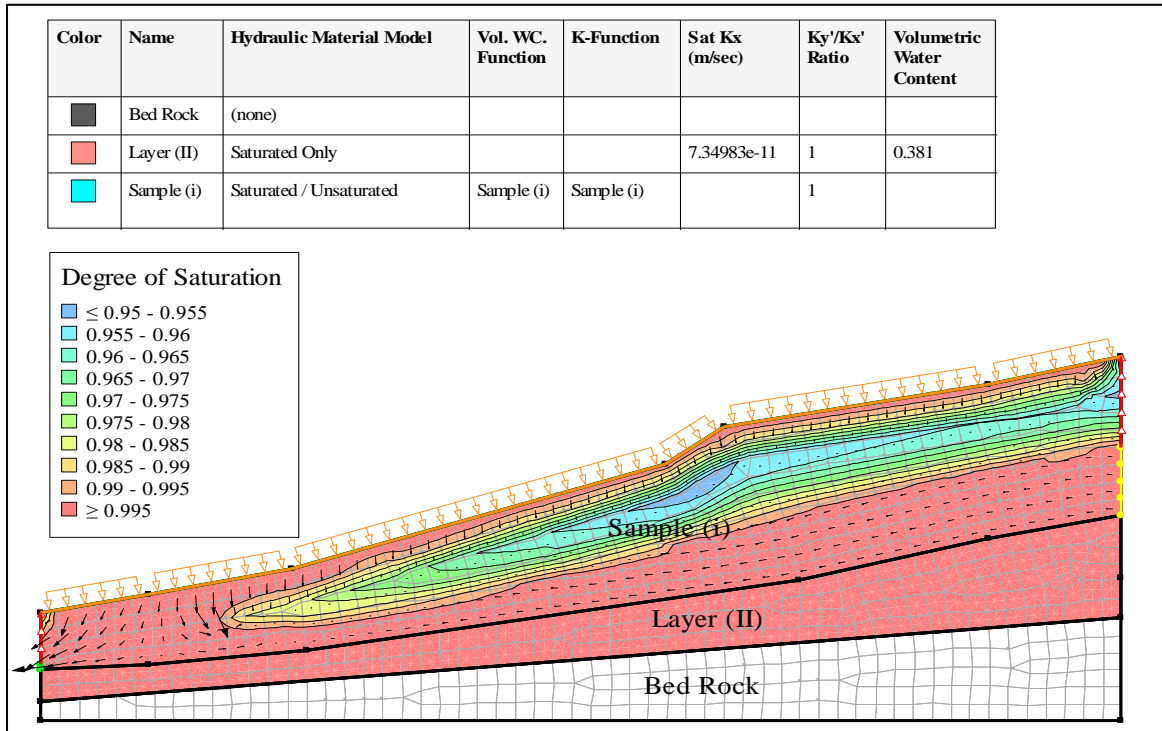
- presentation]. IOP Conference Series: Materials Science and Engineering. IOP Publishing. <https://doi.org/10.1088/1757-899X/527/1/012016>
- Bernama. (2021). *Ranau-Sandakan Road closed due to landslide*, *Daily Express*. Retrieved from <https://www.dailyexpress.com.my/news/206650/ranau-sandakan-road-closed-due-to-landslide/>
- Bernama. (2022). *Repair works on Sandakan Road damaged by landslide to begin next month - Bung Moktar*, *BERNAMA*. Retrieved from <https://www.bernama.com/en/news.php?id=2091213>
- Bishop, A. W., & Henkel, D. J. (1962). *The Measurement of Soil Properties in the Triaxial Test* (2nd Ed.). London, UK: Edward Arnold (Publishers) LTD.
- Borneo Post Online. (2023). *Ranau-Sandakan Road closed due to landslide, says Sabah JKR*, *Borneo Post Online*. Retrieved from <https://www.theborneopost.com/2023/01/30/ranau-sandakan-road-closed-due-to-landslide-says-sabah-jkr/>
- BS 1377, B. S. (1990). Methods of test for soils for civil engineering purposes. *British Standards Institution. London. UK*.
- Cao, L., Wang, Z., & Chen, Y. (2016). Unsaturated seepage analysis of cracked soil including development process of cracks. *Advances in Materials Science and Engineering*, 2016(1), Article 2684297. <https://doi.org/10.1155/2016/2684297>
- Carvalho, J. C. D., & Gitirana Jr, G. D. F. (2021). Unsaturated soils in the context of tropical soils. *Soils and Rocks*, 44(3), Article e2021068121. <https://doi.org/10.28927/SR.2021.068121>
- Chung, K. W., Sum, C. W., & Rahman, A. H. A. (2015). Stratigraphic succession and depositional framework of the Sandakan formation, Sabah. *Sains Malaysiana*, 44(7), 931-940. <https://doi.org/10.17576/jsm-2015-4407-03>
- Cornelis, W. M., Khlosi, M., Hartmann, R., Van Meirvenne, M., & De Vos, B. (2005). Comparison of unimodal analytical expressions for the soil-water retention curve. *Soil Science Society of America Journal*, 69(6), 1902-1911. <https://doi.org/10.2136/sssaj2004.0238>
- Das, B. M., & Sivakugan, N. (2019). *Principle of Foundation Engineering* (9th Ed.). Cengage Learning.
- Esmaeelnejad, L., Ramezanpour, H., Seyedmohammadi, J., & Shabanpour, M. (2015). Selection of a suitable model for the prediction of soil water content in north of Iran. *Spanish Journal of Agricultural Research*, 13(1), 1–11. <https://doi.org/10.5424/sjar/2015131-6111>
- Fan, C. C., & Zeng, R. Y. (2016). Effect of characteristics of unsaturated soils on the stability of slopes subject to rainfall. *Japanese Geotechnical Society Special Publication*, 2(29), 1060–1064. <https://doi.org/10.3208/jgssp.TWN-02>
- Fathiyah, H. S., & Bahsan, E. (2016, November 9-12). *Parametric study on the effect of rainfall pattern to slope stability* [Conference presentation]. Sriwijaya International Conference on Engineering, Science and Technology (SICEST 2016), Bangka Island, Indonesia. <https://doi.org/10.1051/mateconf/201710105005>
- Fell, R., MacGregor, P., Stapledon, D., & Bell, G. (2005). *Geotechnical Engineering of Dams*. London, UK: Taylor & Francis Group plc.
- Fredlund, D. G., & Xing, A. (1994). Equations for the soil-water characteristic curve. *Canadian Geotechnical Journal*, 31(4), 521–532. <https://doi.org/10.1139/t94-061>
- Fredlund, D. G., & Fredlund, M. D. (2020). Application of ‘estimation procedures’ in unsaturated soil mechanics. *Geosciences (Switzerland)*, 10(9), Article 364. <https://doi.org/10.3390/geosciences10090364>
- Garcia Aristizabal, E. F., Riveros Jerez, C. A., & Builes Brand, M. A. (2011). Influence of rainfall intensity on infiltration and deformation of unsaturated soil slopes. *Dyna*, 78(170), 116-124.
- GEO-SLOPE International, L. (2023). Stability Modeling with GeoStudio. In *GeoStudio*. GeoStudio, Seequent.
- Habasimbi, P., & Nishimura, T. (2019). Soil Water Characteristic Curve of an Unsaturated Soil under Low Matric Suction Ranges and Different Stress Conditions. *International Journal of Geosciences*, 10(01), 39–56. <https://doi.org/10.4236/ijg.2019.101004>
- Harisuseno, D., & Cahya, E. N. (2020). Determination of soil infiltration rate equation

- based on soil properties using multiple linear regression. *Journal of Water and Land Development*, 47(1), 77–88.
<https://doi.org/10.24425/jwld.2020.135034>
- Huong, N. T. N., & Thu, T. M. (2024). Characteristic of Unsaturated Soil of Earth Fill Dams in Vietnam. *Geotechnical Engineering Journal of the SEAGS & AGSSEA*, 47(1), 106–117.
<https://doi.org/10.14456/seagj.2016.66>
- Izumi, T., Matsuura, S., Mohd Yusof, A. F., Razak, K. A., Moriguchi, S., Kure, S., ... & Supar, L. (2019). Disaster Risk Report: Understanding Landslides and Flood Risks for Science-Based Disaster Risk Reduction in the State of Selangor. *IRIDeS, Japan; Universiti Teknologi Malaysia*, 1.
- John, K. R. (2020). Swelling Clay Minerals and Slope Cut Failures in the Garinono Formation Along Jalan Sungai Hitam, Libaran, Sandakan. *Geological Behavior (GBR)*, 4(1), 29–34.
<https://doi.org/10.26480/gbr.01.2020.29.34>
- Kechik, F. A., Ibrahim, A., Abu Hassan, Z., Matlan, S. J., Taib, A. M., & Rahman, N. A. (2023). Analysis of influence of air-entry values to unsaturated soil properties. *Physics and Chemistry of the Earth*, 129, Article 103340.
<https://doi.org/10.1016/j.pce.2022.103340>
- Khlosi, M., Cornelis, W. M., Douaik, A., van Genuchten, M. T., & Gabriels, D. (2008). Performance Evaluation of Models That Describe the Soil Water Retention Curve between Saturation and Oven Dryness. *Vadose Zone Journal*, 7(1), 87–96.
<https://doi.org/10.2136/vzj2007.0099>
- Kumar, S., & Roy, L. B. (2023). Experimental and Numerical Analysis of Unsaturated Soil Slope Stability with Rainfall and Jute Fibre Reinforcement Condition. *Geotechnical Engineering Journal of the SEAGS & AGSSEA*, 54(1), 15–32.
<https://doi.org/10.14456/seagj.2023.23>
- Leong, E. C., & Rahardjo, H. (1997a). Permeability Functions for Unsaturated Soils. *Journal of Geotechnical and Geoenvironmental Engineering*, 123(12), 1118–1126.
[https://doi.org/10.1061/\(ASCE\)1090-0241\(1997\)123:12\(1118\)](https://doi.org/10.1061/(ASCE)1090-0241(1997)123:12(1118))
- Leong, E. C., & Rahardjo, H. (1997b). Review of Soil-Water Characteristic Curve Equations. *Journal of Geotechnical and Geoenvironmental Engineering*, 123(12), 1106–1117.
[https://doi.org/10.1061/\(ASCE\)1090-0241\(1997\)123:12\(1106\)](https://doi.org/10.1061/(ASCE)1090-0241(1997)123:12(1106))
- Liu, C., & Evett, J. B. (2008). *Soils and foundations* (7th Ed.). New Jersey, US: Prentice Hall.
- Liu, Y., Deng, Z., & Wang, X. (2021). The effects of rainfall, soil type and slope on the processes and mechanisms of rainfall-induced shallow landslides. *Applied Sciences*, 11(24), Article 11652. <https://doi.org/10.3390/app112411652>
- Look, B. G. (2014). *Handbook of geotechnical investigation and design tables*. (2nd Ed.). Milton Park, UK: Taylor & Francis Group, CRcc Press. <https://doi.org/10.1201/b16520>
- Lu, N., & Godt, J. W. (2013). *Hillslope hydrology and stability*. Cambridge, UK: Cambridge University Press.
- Mahmoud, A. I., Hussein, H. A., & Khaled, Z. S. (2021). Numerical Model of Seepage Analysis and Slope Stability for Horan Dam H4 in Iraq. *IOP Conference Series: Materials Science and Engineering*, 1076(1), Article 012089.
<https://doi.org/10.1088/1757-899x/1076/1/012089>
- Malaysia Kementerian Kerja Raya Jabatan Kerja Raya. (2009). *National Slope Master Plan: Kajian Pelan Induk Langkah-Langkah Pembaikan Cerun di Malaysia (Kajian Pelan Induk Cerun Negara) 2009-2023*. Kuala Lumpur, Malaysia: Jabatan Kerja Raya Malaysia
- Malay Mail (2021). *Malay mail, Heavy rain: Jalan Buli Sim Sim in Sandakan closed due to landslide*. Retrieved from <https://www.malaymail.com/amp/news/malaysia/2021/01/11/heavy-rain-jalan-buli-sim-sim-in-sandakan-closed-due-to-landslide/1939406>.
- Matlan, S. J., Taha, N. A., Dullah, S., Taharin, M. R., & Hamza, H. (2021). Analysis of rainfall effect on slope failure in Sabah. *Malaysian Construction Research Journal*, 33(1), 93–100.
- Musta, B., Erfen, H. F. W. S., Karim, A. S. R., Kim, K. W., & Kim, J. H. (2019). Physico-chemical Properties and Mineralogical Identification of Soils from Mélange in Beluran-Sandakan, Sabah, Malaysia. *Journal of Physics: Conference Series*, 1358(1), Article 012073.
<https://doi.org/10.1088/1742-6596/1358/1/012073>
- Nassor, S. H., Matlan, S. J., & Taha, N. A. (2024). Soil-Water Characteristic Curve analysis of silt clay in the Garinono Formation, Sabah. *Transactions on Science and Technology*,

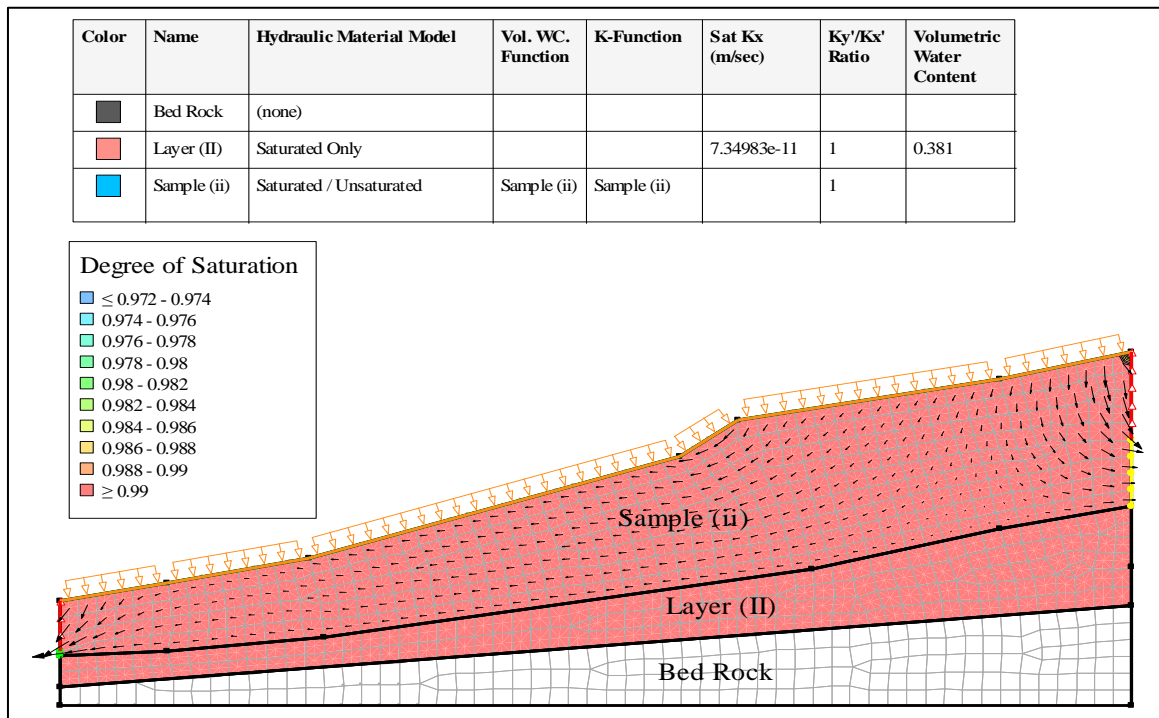
- 11(1), 30–42.
- Ng, C. W. W., Liu, H. W., & Feng, S. (2015). Analytical solutions for calculating pore-water pressure in an infinite unsaturated slope with different root architectures. *Canadian Geotechnical Journal*, 52(12), 1981–1992. <https://doi.org/10.1139/cgj-2015-0001>
- Ng, C. W. W., & Shi, Q. (1998). Influence of rainfall intensity and duration on slope stability in unsaturated soils. *Quarterly Journal of Engineering Geology*, 31(2), 105–113. <https://doi.org/10.1144/GSL.QJEG.1998.031.P2.04>
- Oluyemi-Ayibiowu, B. D., Akinleye, T. O., Fadugba, O. G., & Olowoselu, A. S. (2020). Soil-Water Characteristics of Tropical Clay Soil under High and Low Suction Conditions. *Journal of Geoscience and Environment Protection*, 8(11), 162–175. <https://doi.org/10.4236/gep.2020.811010>
- Pan, Y., Wu, G., Zhao, Z., & He, L. (2020). Analysis of rock slope stability under rainfall conditions considering the water-induced weakening of rock. *Computers and Geotechnics*, 128(999), Article 103806. <https://doi.org/10.1016/j.compgeo.2020.103806>
- Prasad, M. N. V., & Pietrzykowski, M. (Eds.). (2020). *Climate change and soil interactions*. Elsevier.
- Rahardjo, H., Satyanaga, A., & Leong, E. C. (2012). Unsaturated soil mechanics for slope stabilization. *Geotechnical Engineering*, 43(1), 48–58.
- Ray, R., Samui, P., & Roy, L. B. (2023). Reliability analysis of a shallow foundation on clayey soil based on settlement criteria. *Journal of Current Science and Technology*, 13(1), 91–106. <https://doi.org/10.14456/jcst.2023.9>
- Rehan, M., Almani, Z., Ahsan, M., & Jokhio, J. (2024). Numerical Modelling of Matric Suction in Unsaturated Soil under Shallow Foundation Under Varying Soil and Hydrological Conditions. *Jurnal Kejuruteraan*, 36(2), 569–580. [https://doi.org/10.17576/jkukm-2024-36\(2\)-17](https://doi.org/10.17576/jkukm-2024-36(2)-17)
- Research Centre UMS. (2023). *Natural Disaster Research Centre (NDRC), Natural disaster database*. Retrieved from https://ndrc.ums.edu.my/disaster/browse?order=occurrence_date&sort=desc&page=2
- Roslee, R. (2018). Geohazards in Sandakan Town Area, Sabah, Malaysia. *Geological Behavior*, 2(1), 18–23. <https://doi.org/10.26480/gbr.01.2018.18.23>
- Rosly, M. H., Mohamad, H. M., Bolong, N., & Harith, N. S. H. (2022). An overview: relationship of geological condition and rainfall with landslide events at East Malaysia. *Trends in Sciences*, 19(8), 3464–3464.. <https://doi.org/10.48048/tis.2022.3464>
- Sazzad, M. M., Roy, M. R. I. N. M. O. Y., & Rahman, M. M. (2015). FEM based seepage analysis through earth dam. *International Journal of Advances in Structural and Geotechnical Engineering*, 4(3), 158–164.
- Sharratt, B. S. (1990). Water Retention, Bulk Density, Particle Size, and Thermal and Hydraulic conductivity of Arable Soils in Interior Alaska. *Bulletin*, 83.
- Sheng, D., Zhou, A., & Fredlund, D. G. (2009). Shear Strength Criteria for Unsaturated Soils. *Geotechnical and Geological Engineering*, 29(2), 145–159. <https://doi.org/10.1007/s10706-009-9276-x>
- Song, K., Yan, E., Zhang, G., Lu, S., & Yi, Q. (2015). Effect of hydraulic properties of soil and fluctuation velocity of reservoir water on landslide stability. *Environmental Earth Sciences*, 74, 5319–5329. <https://doi.org/10.1007/s12665-015-4541-1>
- State Environmental Conservation Department (ECD), Sabah, Malaysia. (2001). EIA Guideline for Construction on Hillslopes. In L. P. Siong, V. Moduying, Y. Yangkat, T. Greer, C. Hollaender, & E. Juin (Eds.), *The Environmental Conservation Department, Sabah, Malaysia Photos* (Issue 1, p. 72).
- The European Union. (1997). Eurocode 7 - Geotechnical design - Part 2: Ground investigation and testing. Retrieved from <https://www.phd.eng.br/wp-content/uploads/2015/02/en.1997.2.2007-1.pdf>
- Tao, G., Chen, Y., Xiao, H., Chen, Y., & Peng, W. (2020). Comparative Analysis of Soil-Water Characteristic Curve in Fractal and Empirical Models. *Advances in Materials Science and Engineering*, 2020(1), Article 1970314. <https://doi.org/10.1155/2020/1970314>
- White, S. E. (2018). Physical geology. *Journal of Geological Education*, 6(2). <https://doi.org/10.5408/0022-1368-6.2.28a>
- Xi, Y., Guo, C., Li, J., Zhang, Y., & Yang, S. (2021, May 21–23). *A method for determining unsaturated strength parameters in stability analysis of loess slope* [Conference

- presentatuon]. 2021 2nd International Academic Conference on Energy Conservation, Environmental Protection and Energy Science (ICEPE 2021), Dali, China. <https://doi.org/10.1051/e3sconf/202127102005>
- Xue, K., Ajmera, B., Tiwari, B., & Hu, Y. (2016). Effect of long duration rainstorm on stability of Red-clay slopes. *Geoenvironmental Disasters*, 3(1), Article 12. <https://doi.org/10.1186/s40677-016-0046-9>
- Yamusa, Y. B., Hezmi, M. A., Ahmad, K., Kassim, K. A., Sa'ari, R., Alias, N., ... & Rashid, A. S. A. (2019, May 18-22). *Soil water characteristic curves for laterite soil at different water contents and methods as lining system* [Conference presentation]. IOP Conference Series: Materials Science and Engineering. IOP Publishing. <https://doi.org/10.1088/1757-899X/527/1/012002>
- Yang, S. R., & Huang, L. J. (2023). Infiltration and failure behavior of an unsaturated soil slope under artificial rainfall model experiments. *Water*, 15(8), Article 1599. <https://doi.org/10.3390/w15081599>
- Yang, R., Xiao, P., & Qi, S. (2019). Analysis of slope stability in unsaturated expansive soil: a case study. *Frontiers in Earth Science*, 7, Article 292. <https://doi.org/10.3389/feart.2019.00292>
- Yuan, B., Cai, Z., Lu, M., Lv, J., Su, Z., & Zhao, Z. (2020). Seepage analysis on the surface layer of multistage filled slope with rainfall infiltration. *Advances in Civil Engineering*, 2020, Article 8879295. <https://doi.org/10.1155/2020/8879295>
- Yunusa, G. H., Kassim, A., & Gofar, N. (2014). Effect of soil layering on suction distribution in unsaturated residual soil slope. *Electronic Journal of Geotechnical Engineering*, 19, 9351–9376.
- Zaky, F. A., & Seboong, O. (2017). Transient Analysis on Infiltration and Stability for Unsaturated Soils in Busan Landslide Area. *International Journal of Environmental Science*, 2(1), 40–44.
- Zhai, Q., & Rahardjo, H. (2011). Determination of soil - water characteristic curve variables. *Computers and Geotechnics Journal*, 42, 37–43. <https://doi.org/10.1016/j.compgeo.2011.11.010>
- Zhai, Q., & Rahardjo, H. (2015). Estimation of permeability function from the soil-water characteristic curve. *Engineering Geology*, 199, 148–156. <https://doi.org/10.1016/j.enggeo.2015.11.001>
- Zhai, Q., Rahardjo, H., & Satyanaga, A. (2017). Effects of residual suction and residual water content on the estimation of permeability function. *Geoderma*, 303, 165–177. <https://doi.org/10.1016/j.geoderma.2017.05.019>
- Zhao, W., Zhou, C., Hu, J., Ma, F., & Wang, Z. (2022). Soil-Water Characteristic Curves and Fitting Models of Collapsible Loess : A Case Study of Lanzhou , China. *Polish Journal of Environmental Studies*, 31(4), 3455–3462. <https://doi.org/10.15244/pjoes/145412>
- Zhou, J., & Qin, C. (2022). Stability analysis of unsaturated soil slopes under reservoir drawdown and rainfall conditions: steady and transient state analysis. *Computers and Geotechnics*, 142, Article 104541. <https://doi.org/10.1016/j.compgeo.2021.104541>

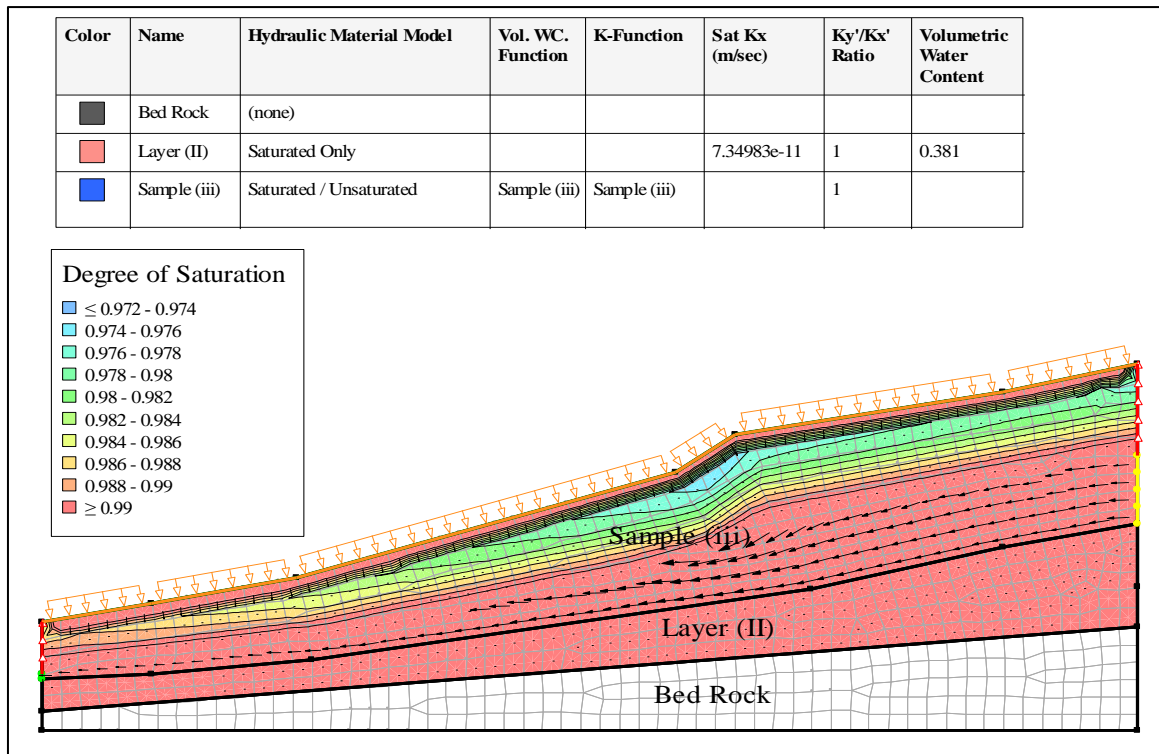
8. Appendix



(a)

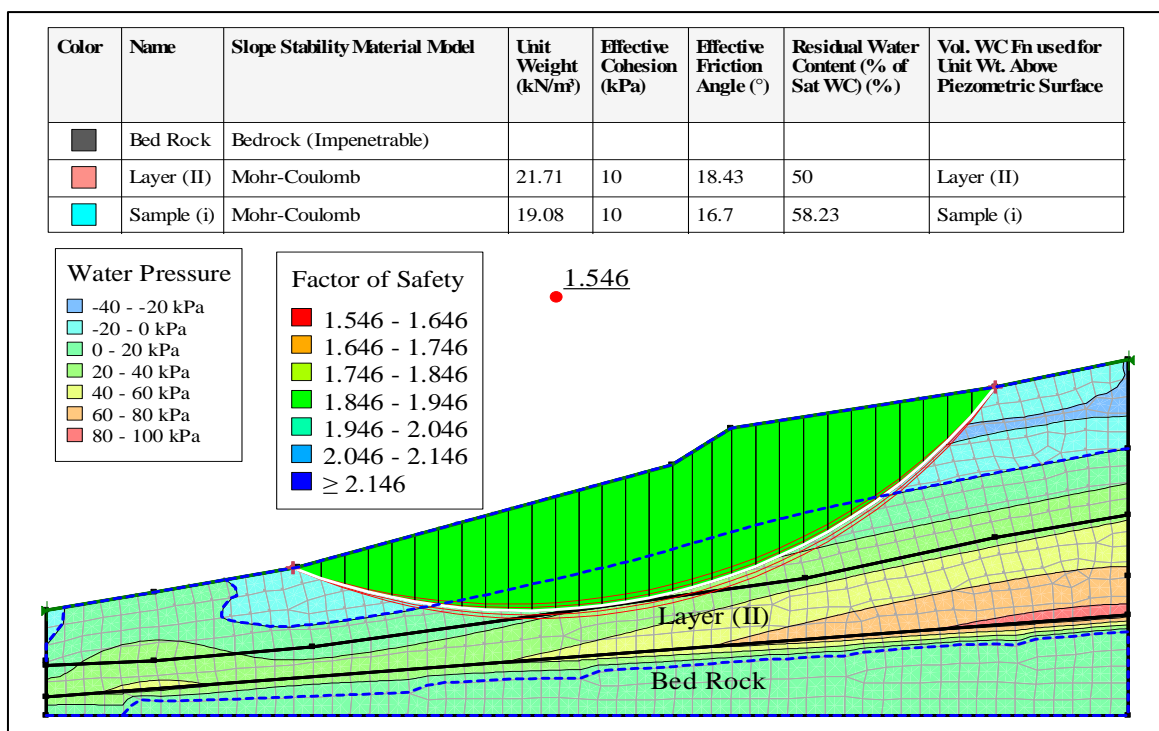


(b)

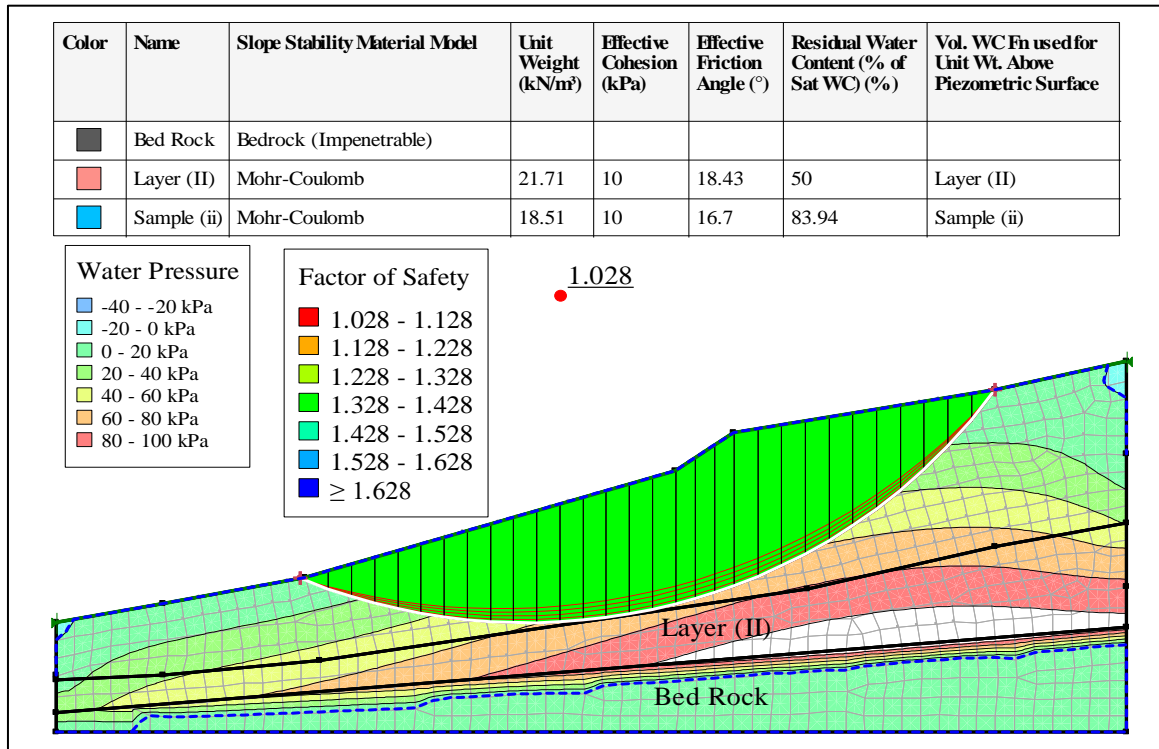


(c)

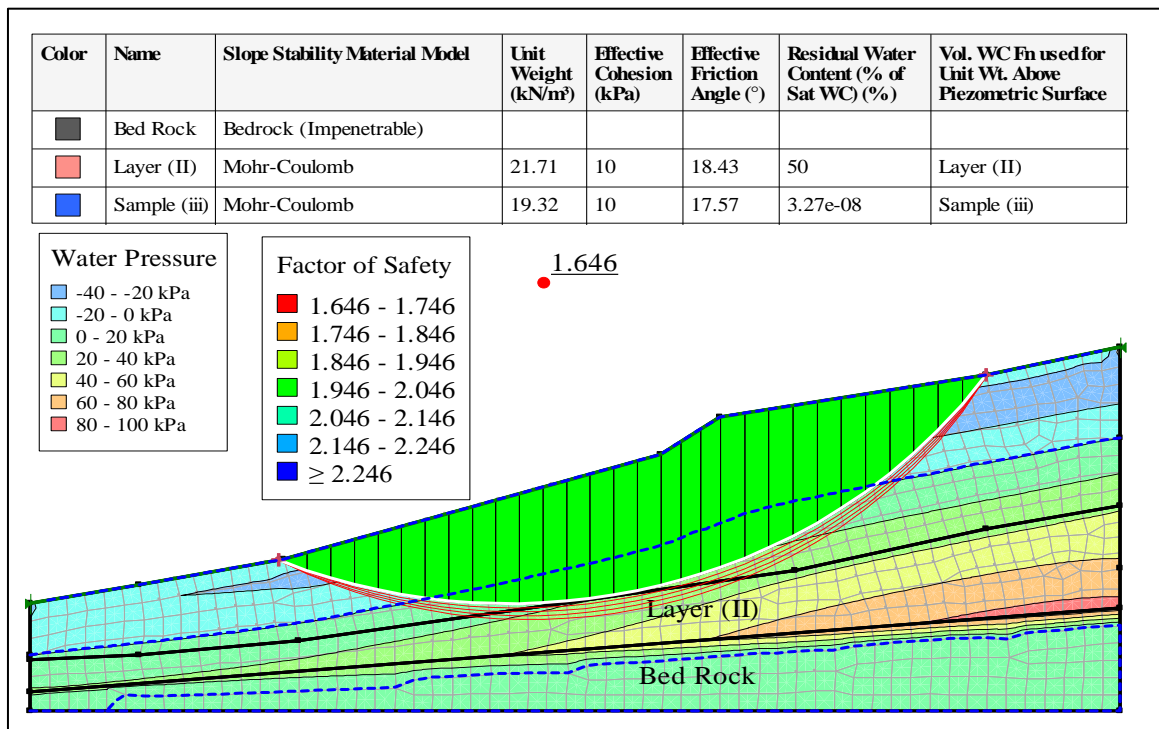
Figure A1 GeoStudio Figures: Degree of Saturation during 31 days of rainfall:(a) Sample (i); (b) Sample (ii); (c) Sample (iii)



(a)



(b)



(c)

Figure A2 GeoStudio Figures: PWP Development and FS during 31 days of rainfall:(a) Sample (i); (b) Sample (ii); (c) Sample (iii)